

Article

Near-Surface Geophysical Characterization of Lithologies in Corfu and Lefkada Towns (Ionian Islands, Greece)

John D. Alexopoulos ¹, Nicholas Voulgaris ¹, Spyridon Dilalos ^{1,*}, Vasileios Gkosios ¹, Ioannis-Konstantinos Giannopoulos ¹, Georgia S. Mitsika ¹, Emmanuel Vassilakis ², Vassilis Sakkas ¹ and George Kaviris ¹

¹ Section of Geophysics and Geothermy, Department of Geology and Geoenvironment, National and Kapodistrian University of Athens, Panepistimioupoli Zografou, 15784 Athens, Greece

² Remote Sensing Laboratory, Department of Geology and Geoenvironment, National and Kapodistrian University of Athens, Panepistimioupoli Zografou, 15784 Athens, Greece

* Correspondence: sdilalos@geol.uoa.gr

Abstract: Lefkada and Corfu old towns are located in the western part of Greece, in the Ionian Sea. Their proximity to the Hellenic subduction zone (HSZ) is the reason for their intense seismicity. The main goal of this study was the estimation of the geotechnical characteristics of the subsurface, with the contribution of applied geophysical techniques. Therefore, seismic refraction tomography (SRT) and multichannel analysis of surface waves (MASW) were applied. A total of thirty-three (33) seismic and geoelectrical profiles were performed in both towns in order to evaluate the geotechnical characteristics of the subsurface formations. Additionally, subsurface resistivity distributions were investigated with the application of electrical resistivity tomography (ERT). Some important elastic moduli were calculated through the combination of estimated seismic wave velocities and laboratory density measurements. The horizontal distribution of seismic velocities and mechanical properties (σ , E , K , G) of Corfu town was illustrated in maps, for the depth of 5 m. The geophysical interpretation also revealed that Lefkada's subsurface consists of only one compact geological formation, with little or no variation of its geophysical-geotechnical characteristics. Beyond that, the ground type classifications for the two towns were determined according to the European Committee for Standardization Eurocode 8, based on V_{S30} values.

Keywords: SRT; MASW; ERT; elastic moduli; urban geophysics



Citation: Alexopoulos, J.D.; Voulgaris, N.; Dilalos, S.; Gkosios, V.; Giannopoulos, I.-K.; Mitsika, G.S.; Vassilakis, E.; Sakkas, V.; Kaviris, G. Near-Surface Geophysical Characterization of Lithologies in Corfu and Lefkada Towns (Ionian Islands, Greece). *Geosciences* **2022**, *12*, 446. <https://doi.org/10.3390/geosciences12120446>

Academic Editors: Feng Cheng and Jesus Martinez-Frias

Received: 31 October 2022

Accepted: 30 November 2022

Published: 3 December 2022

Publisher's Note: MDPI stays neutral with regard to jurisdictional claims in published maps and institutional affiliations.



Copyright: © 2022 by the authors. Licensee MDPI, Basel, Switzerland. This article is an open access article distributed under the terms and conditions of the Creative Commons Attribution (CC BY) license (<https://creativecommons.org/licenses/by/4.0/>).

1. Introduction

The towns of Corfu and Lefkada are the capitals of the homonymous Ionian islands, located in western Greece, across the Ionian Sea. The island of Lefkada is considered to be one of the most active tectonic areas in Europe and in the eastern Mediterranean region due to the existence of the Hellenic Trench (west of the island) that is responsible for the majority of severe earthquakes generated in the area [1]. In the past, Lefkada town experienced severe damage from severe earthquakes; the most recent are the ones of 17 November 2015 ($M_w = 6.5$) and 14 August 2003 [1–6]. On the other hand, Corfu town does not suffer to the same degree from earthquakes, but there has also been damage due to some disastrous earthquakes in the past [7]. Based on [8], the maximum historical intensity value for Lefkada is 8.0 and for Corfu 7.0. Both towns have traditional buildings (old towns) which are quite susceptible to damage.

The amplitude and frequency of the seismic waves' propagation can be significantly affected by near-surface conditions of the subsurface. The geotechnical characteristics of the subsurface across the study area determine these conditions. Nowadays, geophysical investigations can provide useful data on geotechnical characteristics by applying methods such as electrical resistivity tomography (ERT), seismic refraction tomography (SRT), multi-

channel analysis of surface waves (MASW) and ambient noise measurements [9–15]. These methods are fast, relatively inexpensive and nondestructive.

Due to severe damage from the most recent earthquakes close to Lefkada's town in 2003 and 2015, several studies have been published dealing with the seismic response of the town [16–19]. Valuable data for the validation of the geophysical measurements and their interpretation have been retrieved from these publications. The authors of [19] mention the execution of thirteen (13) boreholes performed by the Central Research Institute (CRI) of the Ministry of Public Works after the earthquake of 2015, from which the authors have calculated the V_{S30} of the formations. Their data provided the subsoil characteristics for the waterfront and north district areas of the old town area. Five categories were identified by [19]: artificial deposits, clay ($V_{S30} = 187$ m/s), sand ($V_{S30} = 236$ m/s), sandy silt ($V_{S30} = 270$ m/s) and marl ($V_{S30} = 470$ m/s). Stiff marl of unknown thickness is observed at each site at depths ranging between 15 and 20 m. Additionally, [20] presents the marl as the seismic bedrock of the old town, with $V_S = 550$ m/s, based on seismic profiling. The authors of [16] provide valuable information from geotechnical boreholes in the old town that were executed after the earthquake of 2003 but also from older technical studies. More specifically, they mention that artificial deposits form the top layer, with thickness of 0.5–5 m. Underlying them, clays, sandy clays, clayey sands and sands with gravels are located down to depths of 8–12 m, except for the marina and channel areas, where their bottom extends down to 15–16 m depth. Further, [16] mention a $V_{S30} = 150$ –380 m/s for these formations. Finally, beneath all these formations, the stiff clayey marl, with $V_{S30} = 800$ m/s, is located and extends down to at least 50 m depth.

The geotechnical characteristics of existing geological formations in the towns of Corfu and Lefkada were determined in this paper using near-surface geophysical measurements, which provided essential subsurface distribution of their physical parameters. At the two cities' selected sites, ERT, SRT and MASW techniques were used. The locations were chosen in order to collect the necessary information from each geological formation of these towns.

2. Geological Setting

The subsurface structures of the islands of Corfu and Lefkada are a result of the external plate of the Hellenides [21] and, more specifically, the Ionian and Paxoi tectono-stratigraphic units [22,23], which are comprised mostly of carbonate sediments and several facies of clastic sediments [24].

2.1. Corfu Town

The greater area of Corfu town is mainly structured by five different geological formations, either alpine or post-alpine. Based on [25], the deeper alpine geological formation of the island is the Pantocrator limestones (*Ji k*), with restricted surficial development. They are unpaved, crystalline and in some cases dolomitized or fragmented. Their maximum thickness is almost 60 m. Along with them, the Sinion limestones can be observed in some locations, with interlaid flints. The Viglae limestones (*Js Ks k*) are overlying the Pantocrator-Sinion limestones, which also have interlaid flints.

Regarding the post-alpine formations, the base breccia (*M sc*) are located at the lower horizons, alternating with marls. Overlying them, a package of marls (*M m.st*) with interbedding sandstone and conglomerates exists. In the town of Corfu specifically, the Miocene starts with conglomerate limestones. The town is covered by alluvial deposits, uncomfortably deposited either on the Miocene layers or the alpine formations. The Upper Miocene-Lower Pliocene deposits in Corfu were investigated further by [26] for their hydrocarbon potentiality.

Figure 1 depicts a modified geological map of Corfu town based on the authors' new geological field mapping (at the local scale) that was completed concurrently with the acquisition of geophysical measurements.

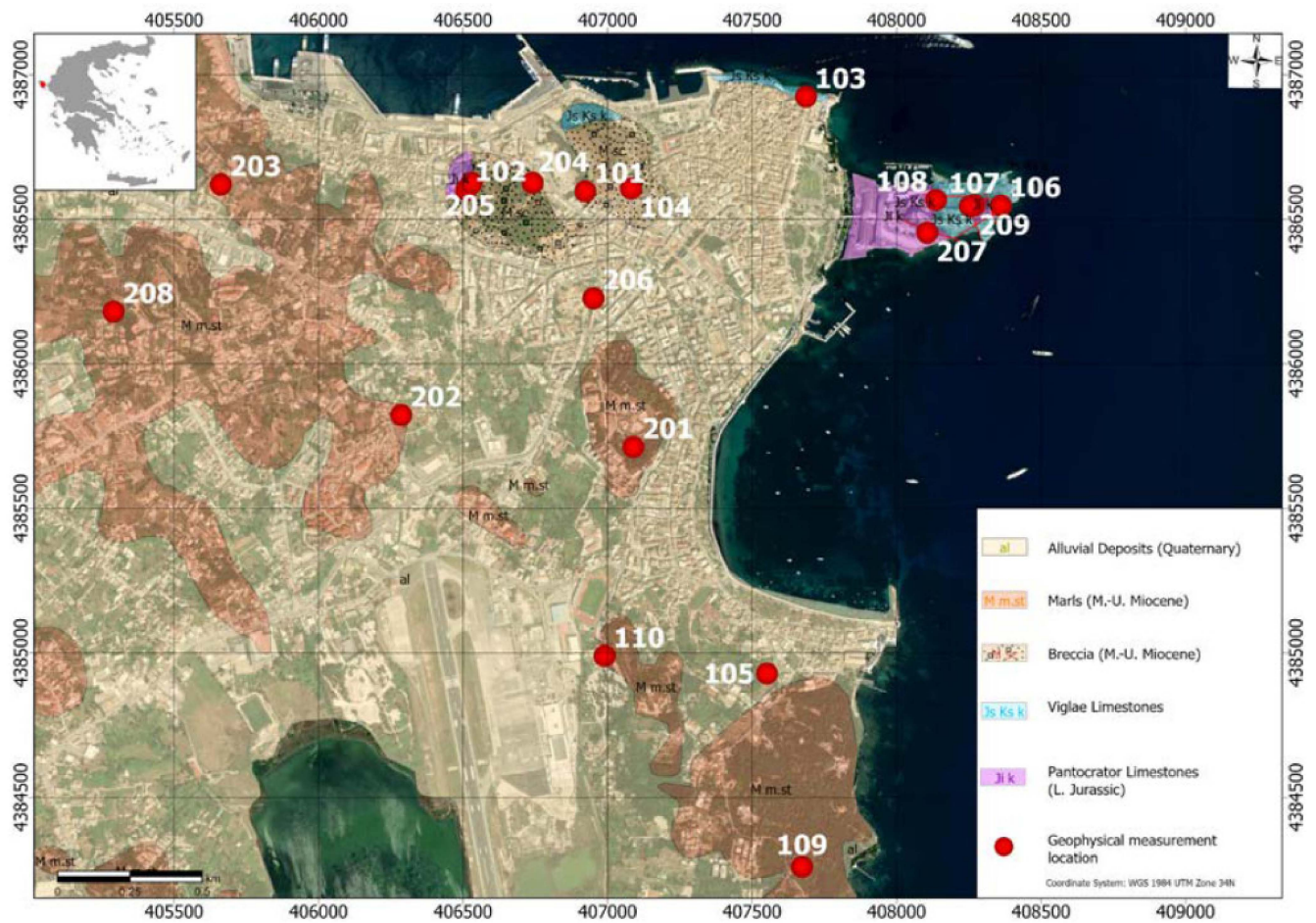


Figure 1. Modified geological map of Corfu town [25].

2.2. Lefkada Town

Geologically, Lefkada town is structured mostly by post-alpine sediments, which are distinguished by more facies than the ones in Corfu town [27,28]. The Ionian unit is considered to be the para-autochthonous unit of Lefkada island, while the *Paxoi* is the relatively autochthonous one, because of minor horizontal displacement that resulted from the alpine deformation phase. The *Paxoi* unit dominates the western part of the island. The Pantocrator limestones (*T5-J3 k*) are also located in the southwest of Lefkada town as the main alpine formation. Regarding the post-alpine sediments in the town's greater area, the alluvial deposits (al), coastal formation from sand (*al s*), coastal beach rocks (*al c*) and lagoon deposits consist of silt, and organic elements (*be*) are also present. Finally, transgressive Miocene molassic-type deposits of sandstones and marls (*M m*) also exist (Figure 2).

A major fault zone is located at the north boundary between the Pantocrator limestones (*T5-J3 k*) and the post-alpine deposits of the town's suburbs [27,29]. It has a NW–SE direction and based on the preliminary interpretation of geophysical measurements by [30], it seems to extend parallel to the north, buried under the alluvial deposits.

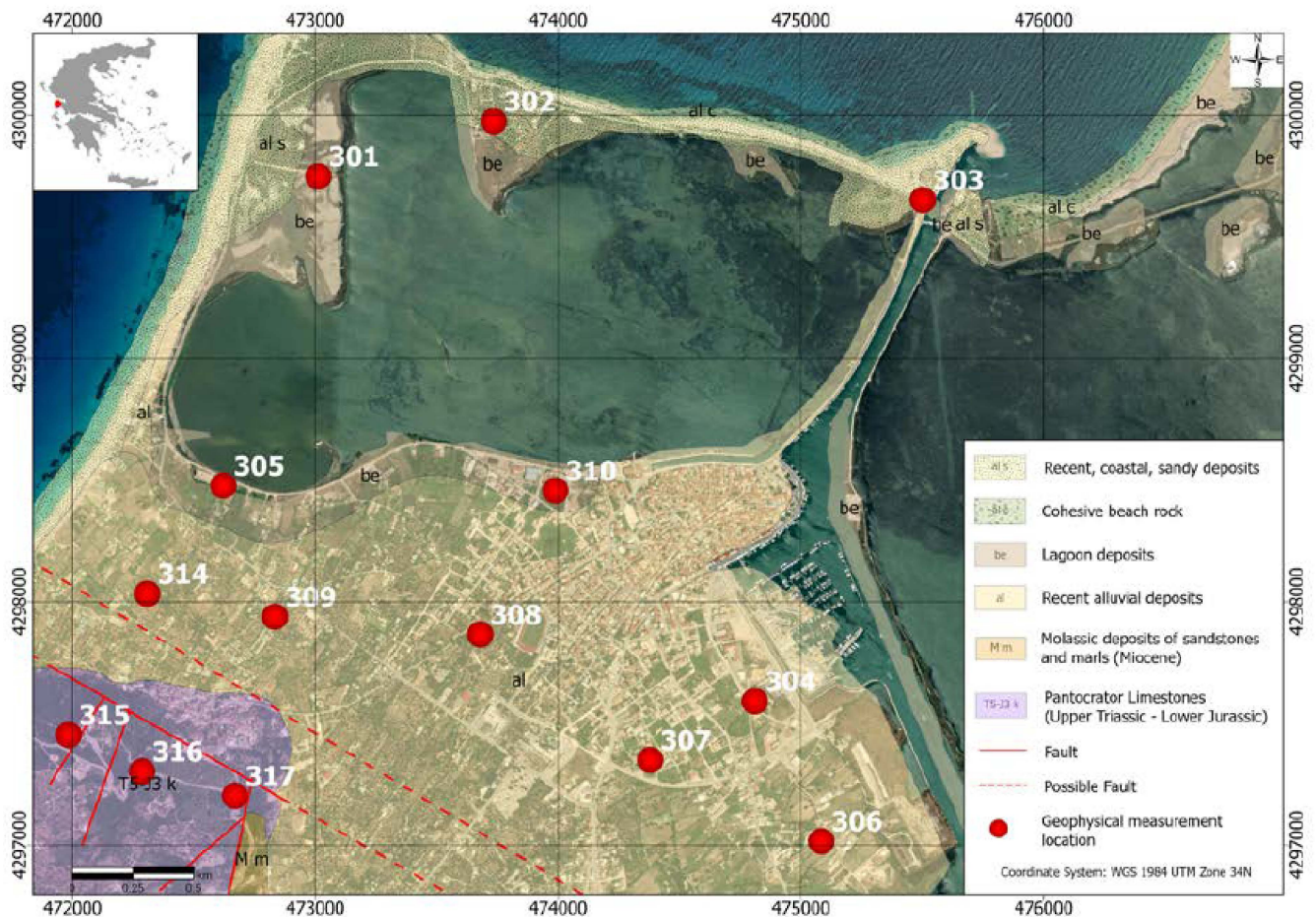


Figure 2. Modified geological map of Lefkada town [31].

3. Methodology

All the geophysical data acquisition was accomplished in three field trips during the first semester of 2022. They were carried out on surficial developments of the geological formations, either alpine or post-alpine, in specific locations as indicated by the red dots in Figures 1 and 2.

In the context of the present geophysical study, at each location, the electrical resistivity tomography (ERT), seismic refraction tomography (SRT) and multichannel analysis of surface waves (MASW) techniques were implemented across the same line.

Thirty-three (33) seismic and electrical sections were carried out in various locations, including nineteen (19) in Corfu town and fourteen (14) in the greater Lefkada town area.

3.1. Seismic Method

By studying the propagation of elastic waves in soil deposits and rocks, many mechanical parameters can be determined. As a result of this, seismic methods, especially the shallow seismic refraction and multichannel analysis of surface waves (MASW) techniques, are quite common in geotechnical applications [12–15].

The shallow seismic refraction technique (SSR) is widely applied for engineering and geotechnical investigations [32–34]. The seismic refraction technique has a low fieldwork cost and good data analysis [35]. More specifically, the seismic refraction tomography (SRT) technique is widely employed to invert seismic refraction data recorded for geotechnical and environmental investigations, and it is known for its constraint across the three-dimensional (3D) distribution of physical properties that obviously has an impact on seismic wave propagation [35–39].

The multichannel analysis of surface waves technique (MASW) has been developed mainly for shallow geophysical investigations to obtain the shear wave velocities and has commonly been used for soil characterization [40–44]. MASW has the advantages of easier fieldwork, detection/recording and processing and is known for its effectiveness and reliability. As [45] indicated, the MASW technique provides reliable shear wave velocity profiles within the first 30 m below the surface.

3.1.1. Data Acquisition

For the estimation of V_P and V_S wave velocities, the 2D seismic refraction tomography (SRT) and 1D multichannel analysis of surface waves (MASW) techniques were implemented, respectively. Both techniques were applied on the same line at a parallel offset to the ERT line. The generation of seismic waves was accomplished using a 6 kg sledgehammer and a metallic plate for better coupling and transmission of the energy through the subsurface to the receivers. Two sets of 24 vertical geophones with natural frequencies of 4.5 and 10 Hz were deployed along each seismic line with 1 m spacing, for the detection of surface and refracted seismic waves, respectively. A 24-channel Geometrics SmartSeis seismograph was used to record the seismic waves with a sampling interval of 0.250 ms and total record length of 512 ms. A total number of 13 shot points were performed at each seismic line, and 3 to 5 stackings were implemented at each shot point in order to minimize the background noise and increase the signal-to-noise ratio. Two of the shot points were performed at a distance of 12 m from the first and last geophones, acting as out shots so as to obtain a record of the critically refracted arrivals along the entire length of the array. Further, two of them were performed at a near offset of 4 m from the first and last geophones to record the surface (Rayleigh) waves. The near offset and spread length distances were determined after several field tests in order to prevent the near- and far-field effects and to ensure the planar development of the surface waves [46]. Lastly, the remaining 9 shot points were performed in between the spread length, with 2.5 to 3 m spacing, in order to ensure an acceptable ray coverage through the medium.

3.1.2. Processing

The acquired seismic refraction data were processed using the *SeisImager/2D* (including *Pickwin* and *Plotrefa*) commercial software package, provided by Geometrics Inc.

The first processing step included the accurate picking of the first break arrivals of the P-waves for each seismic record, using the *Pickwin* module (Figure 3a), obtained by the 13 different shot points. The picked travel times along with the geometric characteristics of the seismic refraction survey, e.g., source location, 1st receiver location and receiver interval, were used to generate the travel time-distance curves for every single seismic line. Afterwards, some travel time curves were edited using the *Plotrefa* module, and the travel time reciprocity between opposite shots was checked for the estimation of P-wave velocity (Figure 3b).

The tomographic inversion process requires an initial velocity model in order to start. Given the fact that there are no borehole data for Corfu town, the authors chose the time-term inversion approach, provided by the *Plotrefa* module, in order to produce a representative initial velocity model. The time-term inversion method employs a combination of linear least squares and delay time analysis in order to invert the first arrivals and generate a velocity section [47]. For the application of this method, layer assignment for each of the first break arrivals (direct or refracted) was performed in the *Plotrefa* module, while the actual elevation of each geophone was defined. Afterwards, an initial 2D discrete-layered velocity model was created, as a result of the inversion process, with each layer being characterized by a unique P-wave velocity value.

The P-wave velocity distribution of the subsurface was determined by applying the tomographic inversion technique. This method starts with the imported initial velocity model and iteratively traces rays through the model with the aim of reducing the RMS error between observed and calculated travel times. The software uses a nonlinear least squares

approach for the inversion step and wavefront propagation methods for the travel time modeling [35,47]. The initial model used was the one derived from the time-term inversion processing technique, which was converted into a grid model. The default inversion parameters, proposed by the software, were used for the inversion process, providing satisfying results. The final outcome of this procedure was a 2D P-wave velocity distribution.

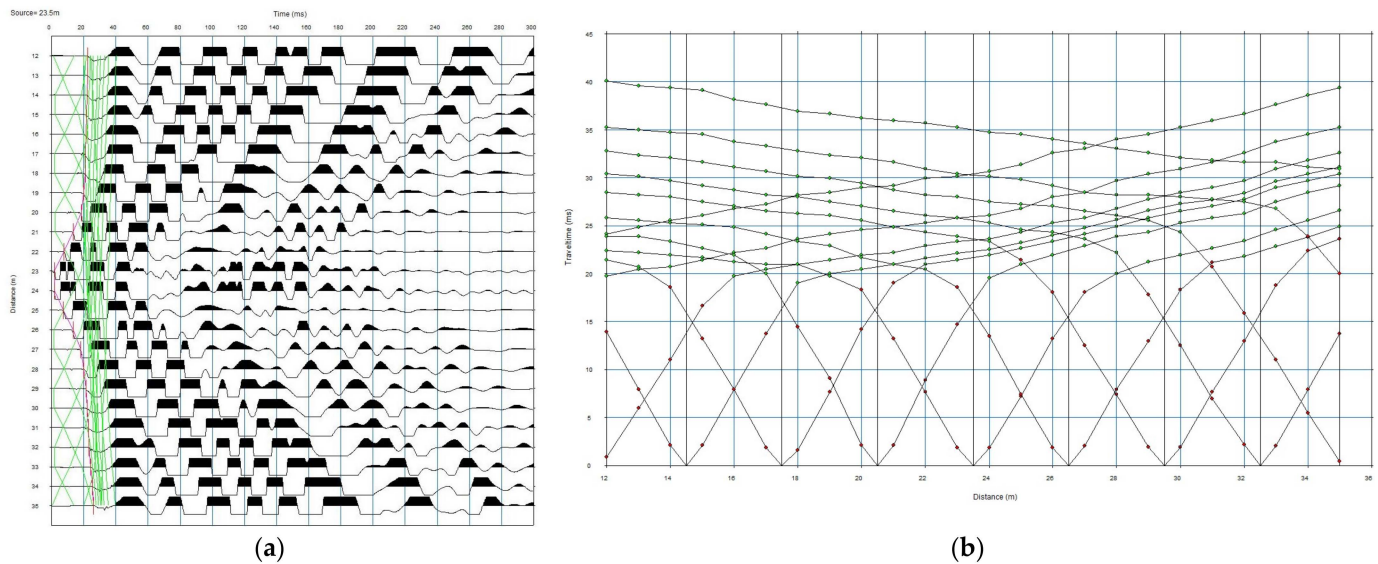


Figure 3. (a) First arrival picking with the shot point located in the middle of the seismic line, (b) P-wave travel time curves of the total 13 shot points along with the first (red dots) and second (green dots) layer assignments.

The MASW method utilizes the dispersive properties of Rayleigh waves to calculate the S-wave velocity distribution through the subsurface by applying a mathematical inversion to the dispersion curve (phase velocity vs. frequency plot). This dispersive property practically means that the propagation velocity (*phase velocity*) of Rayleigh waves depends on the various frequency components of the propagated waves. Therefore, low-frequency components penetrate to greater depths and are characterized by greater phase velocities, while they mainly depend on the elastic properties of the deeper layers [48]. On the other hand, the high-frequency components of surface waves are constrained to shallower layers and thus contain more information about the shallower velocity structure. The processing of seismic records with the active MASW method involves three steps: (i) transformation of the obtained seismic data from the time to frequency domain; (ii) calculation of the dispersion curves and identification of their fundamental mode; and (iii) inversion of the dispersion curves in order to obtain a 1D shear wave velocity distribution to the subsurface.

The acquired seismic data for the 1D active MASW analysis were processed using the *SeisImager/SW (Pickwin and WaveEq)* commercial software package, provided by Geometrics Inc. With the contribution of the *Pickwin* module, the geometry of the seismic experiment was assigned, including the geophone spacing and the distance of the shot to the 1st active receiver (*near offset*). Additionally, some preprocessing steps were conducted in order to improve the quality of the recordings. These steps included the removal of noisy traces and the application of frequency filters in order to suppress the amplitude of body waves and reduce recorded noise. For construction of the dispersion image (Figure 4), the phase shift method, proposed by [49], was applied. The application of this method involves the transformation of multichannel seismic records from the time domain to the frequency domain by applying the fast Fourier transform and calculating the phase velocities of the Rayleigh waves.

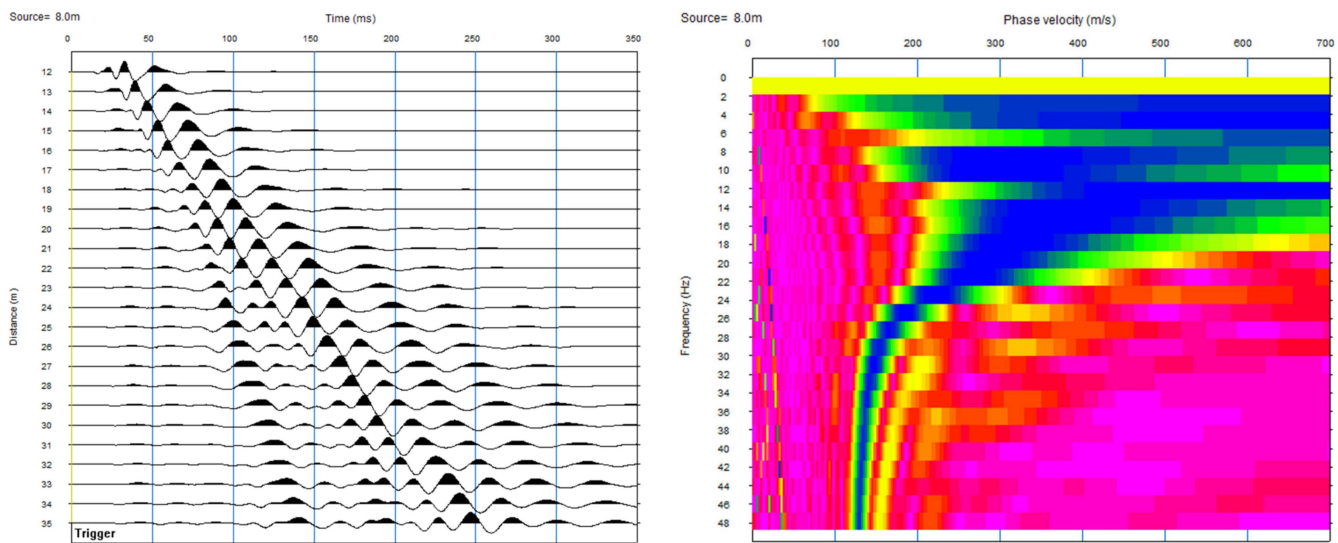


Figure 4. Generation of the dispersion image after transformation of the shot record from the time (left) to the frequency (right) domain.

In the frequency domain, the fundamental mode of the dispersion image was identified, and the dispersion curve was generated by automatically picking the maximum energy amplitude for each frequency at a specified frequency range (4.5–40 Hz). Each pick point corresponds to a phase velocity value at a certain frequency, and all together compose the dispersion curve.

The generated dispersion curves for each measurement site were imported to the *WaveEq* module for further editing, quality checking and processing. Commonly, there are noisy picks on the low- and high-frequency ends of the curve. For that reason, the application of a bandpass filter was considered essential in order to remove those picks and preserve the high-quality part of the curve. Subsequently, a theoretical initial model was calculated based on the *depth conversion result* of the software, as a starting point for the inversion process. Finally, the inversion process was executed using the least squares method, in order to modify the initial model and calculate the V_S curve that best matches the observed data. The final outcome of this procedure was a 1D S-wave velocity distribution that corresponds to the midpoint of each seismic line.

The RMS error for all the 1D V_S final models was less than 6.0 %, providing a high level of confidence.

The V_{S30} value refers to the time-depth-averaged shear wave velocity of the top 30 m of a layered subsurface, and it is calculated by the following equation:

$$V_{S30} = \frac{30}{\sum_{i=1}^N \frac{h_i}{V_i}}$$

where V_i and h_i are the shear wave velocity and thickness of the i -th layer, in a total number of N layers, of the top 30 m of the medium.

According to the National Earthquake Hazards Reduction Program [50] (Table 1), the V_{S30} quantity is used for the classification of a site based on its response to earthquake effects and for the determination of the appropriate seismic-resistant design of buildings.

Table 1. Ground type classification based on [50].

Ground Type	Description of Stratigraphic Profile	V_s^{30} (m/s)
A	Rock or other rock-like geological formation, including at most 5 m of weaker material at the surface.	>800
B	Deposits of very dense sand, gravel or very stiff clay, at least several tens of meters in thickness, characterized by a gradual increase in mechanical properties with depth.	360–800
C	Deep deposits of dense or medium-dense sand, gravel or stiff clay with thickness from several tens to many hundreds of meters.	180–360
D	Deposits of loose-to-medium cohesionless soil (with or without some soft cohesive layers) or of predominantly soft-to-firm cohesive soil.	<180

3.2. Electrical Resistivity Tomography

Electrical resistivity tomography (ERT) is widely used for near-surface investigations and geotechnical applications [9,10] given the fact that both the vertical and horizontal distribution of resistivity, and therefore the respective lithological variations, can be investigated. The authors of [9] support the resistivity method as it is considered to be a more sensitive technique for the variation in subsurface soils than other geophysical techniques.

The Wenner array was chosen, with minimum electrode spacing equal to 1 m, to investigate the subsurface near-surface resistivity distribution for Lefkada and Corfu towns. The instrument used for field measurements was the *IRIS SYSCALPro*. For each electrode along the geoelectrical lines, the coordinates were determined using differential global positioning system (dGPS) and the *GNSS Kolida K5 UFO receiver*. The geodetic system used for the coordinates was the local (Greek) EGSA'87 (Datum GGRS'80).

The acquired resistivity data points were processed with *Res2DInv* Software by Geotomo. During the processing, the software tries to minimize the misfit error of an arbitrary model, checking the raw data points. The inversion process is continuously repeated until the minimum possible misfit is reached.

3.3. Density Determination

Several authors [51–55] have determined the bulk density of geological samples based on laboratory measurements. According to the procedure [56], 3 different measurements of weights are needed: W_1 (dry specimen measured in air), W_2 (saturated specimen measured in air) and W_3 (saturated specimen measured in water). Based on these measurements, the dry bulk density ρ_d , the saturated bulk density ρ_s and the granular one ρ_g can be determined. For near-surface geotechnical purposes, especially above the water table, the appropriate density is usually the dry bulk one. At some of our measurement locations, the water table was located close to the surface, and for that reason we used the saturated density.

For reliable determination of densities, it was proposed to measure several samples from each geological formation and calculate their average characteristic value. Taking this into consideration, the authors carried out laboratory density measurements on 190 geological specimens collected from the locations of the geophysical measurements. The precision scale used was *Kern EMB 100-3* with a readability accuracy of 0.001 gr. In Table 2, the calculated densities of all geological formations from both Lefkada and Corfu towns are presented. Both towns have similar geology, with minor differences mainly in the post-alpine deposits.

Table 2. Density values of each geological formation of Lefkada and Corfu towns.

Geological Formation	Number of Specimens	Dry Density (gr/cm ³)	Saturated Density (gr/cm ³)	Standard Deviation
Breccia (<i>M sc</i>)	60	2.62	2.64	±0.06
Marls (<i>M m.st + M m</i>)	40	1.95	2.19	±0.05
Viglae limestones (<i>Js Ks k</i>)	70	2.66	2.67	0.02
Pantocrator limestones (<i>Ji k+T5-J3 k</i>)	20	2.65	2.69	0.02

4. Interpretation

In this part, an indicative set of seismic and ERT results for each investigated geological formation of Lefkada and Corfu towns is presented. Therefore, for each one of the geological formations, a figure including an SRT profile along its V_{S30} model and the resistivity model from the ERT data is provided. Note that SRT is practically part of the ERT section, and for this reason, the distance axis of the SRT refers to the ERT distance (considering the start of the ERT as the zero point of all the geophysical data). This will lead to a better understanding of their geotechnical characteristics. The processing results of all the seismic and geoelectrical measurements were interpreted based on the gathered geological information (e.g., density measurements, geological maps and boreholes).

4.1. Marl (*M m.st/M m*)

At location 310, the geophysical measurements were carried out on the Upper Miocene marls. The seismic processing results (Figure 5) revealed three seismic layers with the following characteristics: $V_{P1} = 600$ m/s, $V_{P2} = 1200$ m/s, $V_{P3} > 1600$ m/s, and an average thickness of 2.5 m for the first and 2.1 m for the second layer. Regarding the results of the 1D seismic data processing using the MASW technique (Figure 5), two seismic layers were determined, with $V_{S1} = 140$ m/s, thickness 4.2 m and $V_{S2} = 200$ m/s. The average shear wave velocity in the top 30 m was calculated equal to $V_{S30} = 240$ m/s.

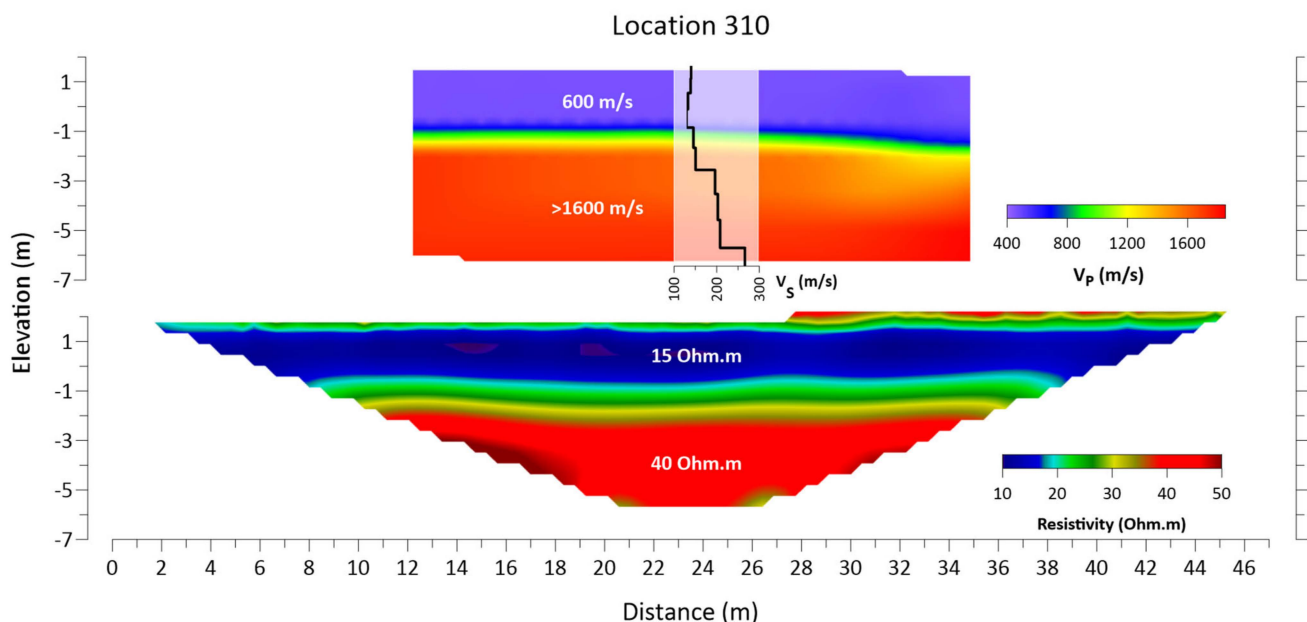


Figure 5. SRT and MASW (top) and ERT (bottom) sections at location 310, investigating the marl formation (*M m.st*).

In Figure 5, the resistivity model from the ERT measurements at location 310 can also be observed. The Upper Miocene marls formation can be related to the relatively resistant geoelectrical layer of 25–50 Ohm·m average resistivity value, which dominates the section at depths greater than 4 m.

The Upper Miocene marl formation is present and has been investigated at both Lefkada and Corfu towns (Figures 1 and 2). The evaluation of all the relative data and results reveals that the values of the geophysical parameters (e.g., V_P and V_S) between the two areas are similar, which leads to the theory that the two geological formations are the same.

4.2. Breccia (*M sc*)

From the processing results of the seismic measurements at location 204, on the breccia formation, three seismic layers were identified (Figure 6). The first layer has an average thickness of 1.5 m and an average velocity of $V_{P1} = 800$ m/s, the second one exhibits thickness close to 2.5 m and $V_{P2} = 1700$ m/s, while the third layer has $V_{P3} > 2000$ m/s. According to the 1D MASW technique, the shear wave velocity of the bedrock greater than 5 m in depth was calculated to 820 m/s. The average shear wave velocity from the surface to a depth of 30 m (V_{S30}) has an estimated value of 950 m/s.

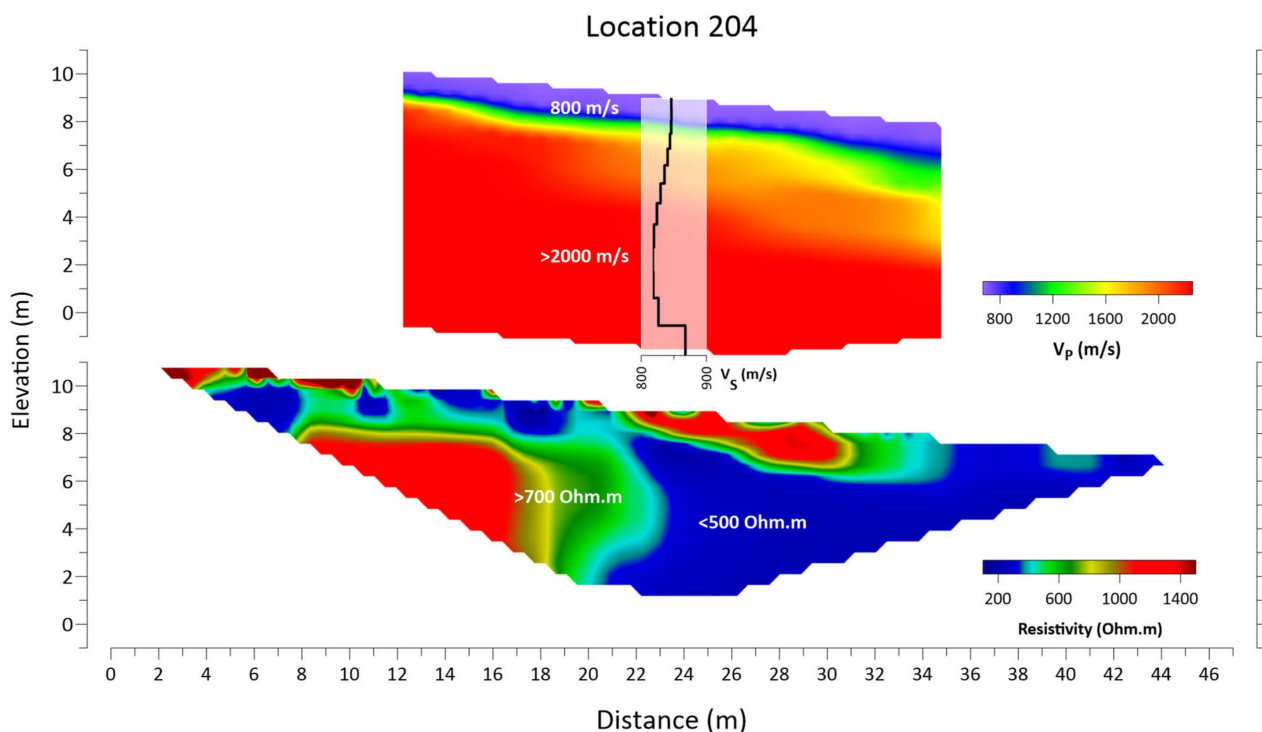


Figure 6. SRT and MASW (top) and ERT (bottom) sections at location 204, investigating the breccia formation (*M sc*).

In the resistivity model of Figure 6 (bottom), relatively resistant zones (>700 Ohm·m) were identified in several parts of the section, corresponding to the consistent parts of the breccia formation. On the other hand, the relatively more conductive zones (<500 Ohm·m) are probably associated with the weathered sections of the breccia formation.

4.3. Viglae Limestone (*Js Ks k*)

The corresponding seismic model (Figure 7), on a surface excursion of the Viglae limestones at location 103, is determined by $V_{P1} = 800$ m/s, $V_{P2} = 1500$ m/s and $V_{P3} > 2500$ m/s, with an average thickness of the first and second layers equal to 2.0 m each. As far as the MASW technique is concerned, one seismic layer can be observed, with average shear wave velocity equal to 1150 m/s. The decrease of the velocity with depth is probably caused by seawater intrusion, due to the proximity of the location to the shore and the permeability of the limestone formation. Additionally, the V_{S30} value was determined equal to 1350 m/s.

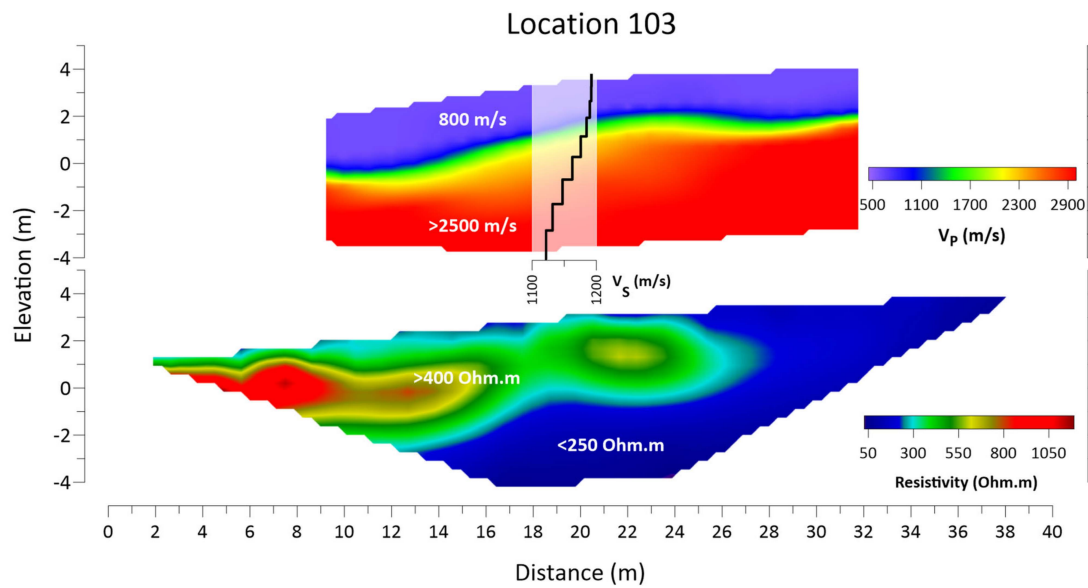


Figure 7. SRT and MASW (top) and ERT (bottom) at location 103, investigating the Viglae limestone (*J_s K_s k*).

In the ERT section (Figure 7), high resistivity values ($>400 \text{ Ohm}\cdot\text{m}$) dominate in the initial and central parts of the section, at depths up to 4 m. On the contrary, a conductive zone ($50\text{--}250 \text{ Ohm}\cdot\text{m}$) appears at greater depths, at the end of the section. The high resistivity values are interpreted as the solid geological formation of the Viglae limestones, while the conductive zone is considered to be caused from the combination of the weathered parts of the limestone and possible seawater intrusion, as mentioned above.

4.4. Pantocrator Limestone (*J_i k*)

The seismic section at location 205 was carried out on the Pantocrator limestones. The processing results (Figure 8) reveal three seismic layers with average velocities $V_{P1} = 900 \text{ m/s}$, $V_{P2} = 1800 \text{ m/s}$ and $V_{P3} > 2300 \text{ m/s}$, and corresponding average thickness equal to 2.2 and 2.0 m for the first and second layers, respectively. Regarding the MASW technique, one seismic layer was identified, with average shear wave velocity equal to 940 m/s and $V_{S30} = 1030 \text{ m/s}$.

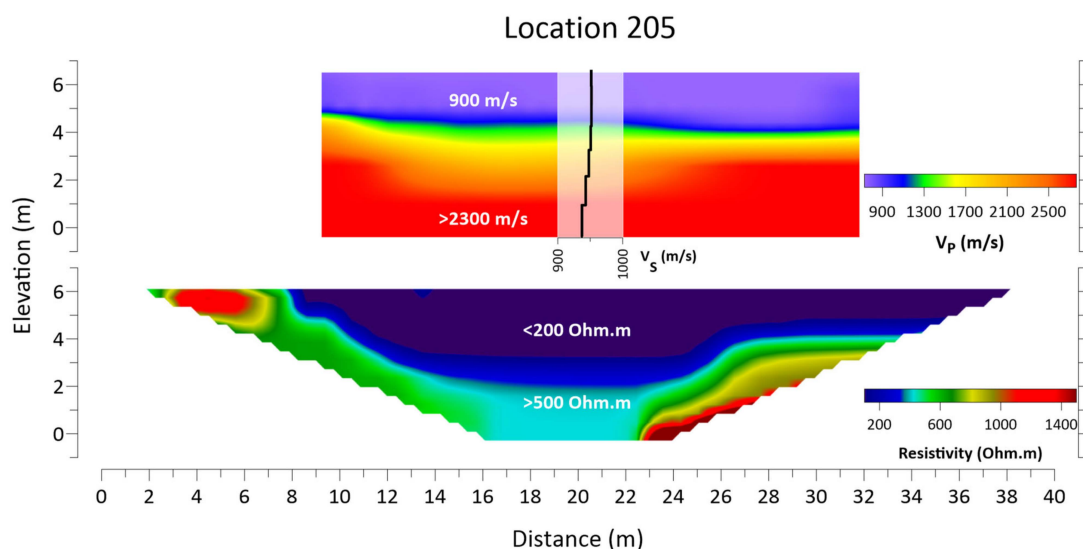


Figure 8. SRT and MASW (top) and ERT (bottom) at location 205, investigating the Pantocrator limestone (*J_i k*).

In the resistivity model (Figure 8), a relatively resistant geoelectrical formation (>500 Ohm·m) can be observed, which is considered to be the solid bedrock of Pantocrator limestones. The structure of the bedrock’s upper boundary in the ERT section is associated very well with the SRT section at this location.

5. Discussion and Elastic Moduli

The calculation approach of elastic moduli with the contribution of geophysical and density measurements has been successfully applied in several older studies for geotechnical purposes [33,57–61].

For the calculation of elastic moduli, the equations listed in Table 3 were used.

Table 3. Elastic moduli equations.

Elastic Modulus	Equation	Reference
Poisson’s ratio (σ)	$\sigma = \frac{1}{2} \left[1 - \frac{1}{(V_P/V_S)^2 - 1} \right]$	[62]
Young’s modulus (E)	$E = \rho \frac{3V_P^2 - 4V_S^2}{(V_P/V_S)^2 - 1}$	[62]
Shear modulus (G)	$G = \frac{E}{2(1+\sigma)}$	[63]
Bulk modulus (K)	$K = \frac{E}{3(1-2\sigma)}$	[63]

Poisson’s ratio (σ) expresses the ratio of the deformation perpendicular to the deformation parallel to the applied stress. It is a nondimensional quantity, and its values range between 0.1 to 0.5 for the compact and loose formations, respectively. Young’s modulus (E) is the ratio between longitudinal stress and longitudinal strain when an elastic solid is exposed under uniaxial compression or extension. Shear modulus (G) is calculated based on the V_s and density values using the simple elastic relationship $G = \rho V_{S2}$, where V_s is the shear wave velocity in m/s, and ρ is the density in g/cm^3 . This parameter is used to define the stiffness matrices for finite element analysis of earth structures and foundation soils. Bulk modulus (K) describes the deformation of the volume of an under-pressure medium.

In the present study, Poisson’s ratio (σ), shear modulus (G), Young’s modulus (E) and bulk modulus (K) have been calculated. For the estimation of the above elastic moduli, V_P and V_S values were calculated using the acquired seismic geophysical profiles (SRT-MASW), while the density values were estimated from laboratory measurements on samples collected from each geological formation of the study area. In Table 4, the median values of all the previously mentioned parameters for every lithological type, along with their classification based on that [50] derived from V_{S30} values, are presented.

Table 4. Seismic velocities and the corresponding elastic moduli and ground types (based on [50]) of the geological formations of Corfu and Lefkada towns.

Geological Formations	V_P (m/s)	V_S (m/s)	V_{S30} (m/s)	Density (g/cm^3)	Poisson’s Ratio, σ	Shear Modulus G (GPa)	Young’s Modulus E (GPa)	Bulk Modulus K (GPa)	ρ (Ohm·m)	Ground Type [50]
Breccia (M sc)	2300	1000	950	2.63	0.40	2.62	7.25	11.89	700	A
Marls (M m.st+M m)	1600	300	240	2.19	0.48	0.19	0.56	5.12	30	C
Viglae limestones (Js Ks k)	2700	1000	1350	2.67	0.39	2.63	7.47	17.20	600	A
Pantocrator limestones (Ji k+T5-J3 k)	2500	930	1030	2.68	0.42	2.29	6.51	14.84	800	A

Many researchers [13,33,42,57,61] present maps with the horizontal distribution of geotechnical parameters and elastic moduli. In Figure 9, the horizontal distribution of seismic velocities and elastic moduli of Corfu town is provided. More specifically, the horizontal distribution is presented at the depth of five (5) meters for V_P (Figure 9a), V_S

(Figure 9b), Poisson’s ratio (σ) (Figure 9c), Young’s modulus (E) (Figure 9d), bulk modulus (K) (Figure 9e) and shear modulus (G) (Figure 9f).

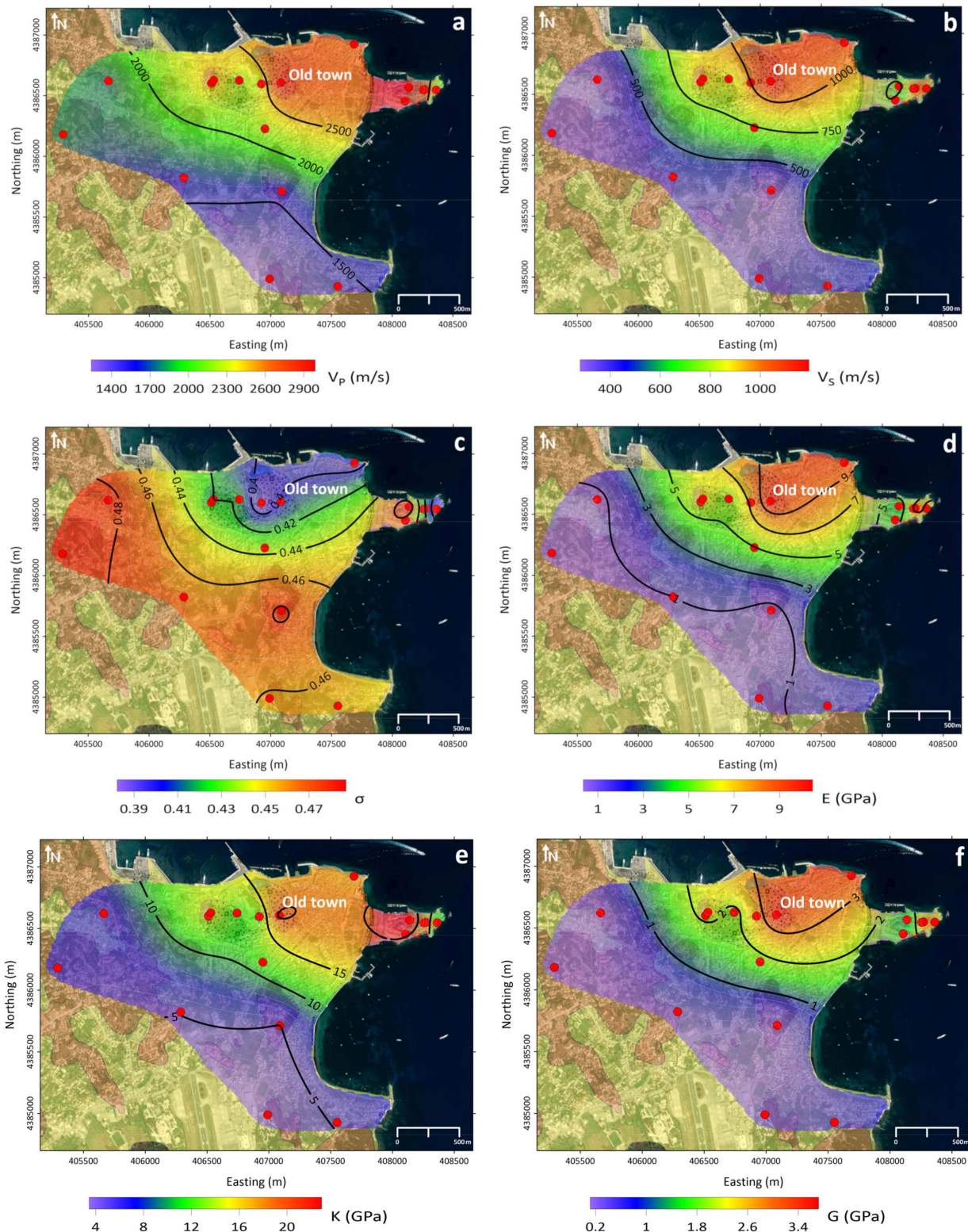


Figure 9. Maps of horizontal distribution of seismic parameters and elastic moduli. (a) V_P , (b) V_S , (c) Poisson’s ratio, (d) Young Modulus, (e) Bulk modulus and (f) Shear modulus at Corfu old town.

In Figure 9a,b, a smooth increase of V_P and V_S , respectively, from the suburbs in the southwestern part of the study area to the old town, located in the northeastern part of the

study area, can be observed. Regarding Poisson's ratio (Figure 9c), a small reduction of its value is observed from the southwestern part to the northeastern part of the study area, indicating that a more solid bedrock is present towards the old town. On the other hand, the Young, bulk and shear moduli (Figure 9d–f) present a corresponding increase along the prementioned direction, regarding their values.

Regarding the town of Lefkada, the formation of marls was investigated at almost all the locations of geophysical measurements. Therefore, given the fact that it is considered an important geological formation for the geotechnical characteristics of the area, the map of Figure 10 was created, illustrating the absolute depth of the marl's roof. It is obvious that the formation of marl dips to the north, as it was investigated at greater depths in the old town than in the northwestern area. The interpretation of geophysical results for the production of this map has been validated based on published geological data, such as important borehole data from the area [16].

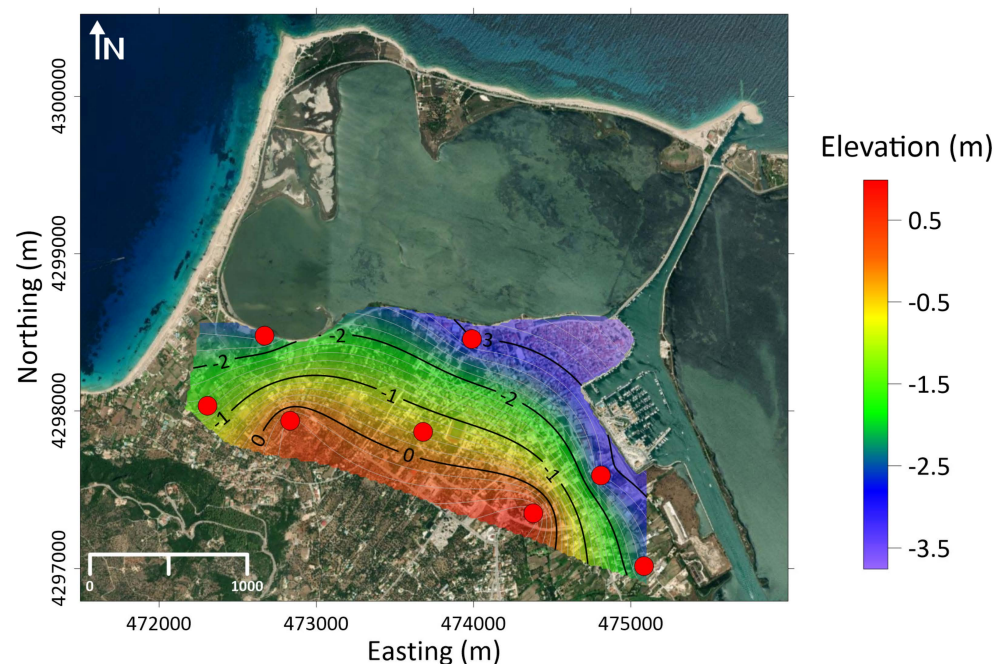


Figure 10. The absolute elevation of marl's roof, based on interpretation of the geophysical measurements from Lefkada old town.

6. Conclusions

The applied geophysical surveys that have been deployed across the areas of the two historical towns of the Ionian islands (Lefkada and Corfu) provided important information regarding the site characterization of their subsurface. More specifically, seismic parameters (e.g., V_P , V_S) and elastic moduli (Poisson's ratio, shear, bulk and Young moduli) of Lefkada and Corfu towns were determined, which can be used for the update of the Greek Antiseismic Regulation of these two areas.

As has already been mentioned, the geology between Lefkada and Corfu towns is structured by the same geological formations (Ionian unit). The only exception concerns the lithology of the marl's formation, at least when it comes to its description in the corresponding geological maps. In Corfu town, the package of marls (*M m.st*) consists of interbedding sandstone and conglomerates while in Lefkada town the Miocene molassic-type deposits of sandstones and marls (*M m*) exist. Based on the geophysical data, it seems that these two formations have the same seismic characteristics.

From the horizontal distributions of the seismic parameters and elastic moduli (Figure 9a–f) and the values of each geological formation (Table 2), the geological boundaries between the marls and the hard rocks (at depth 5 m) can be delineated. This can be placed somewhere along

the contour of $V_p = 2000$ m/s and the contour of $V_s = 500$ m/s, with the soft formation (class D) located southwest (suburbs) and the hard rocks (class B) in the remaining area, including the old town. Additionally, with the aid of resistivity measurements, the marl's roof boundary has been adumbrated (Figure 10), and its dip to the north was also determined, an important factor in the geotechnical behavior of the Lefkada old town.

Based on the European Committee for Standardization Eurocode 8 [50] and the processing results, the geological formations have been classified based on ground types. More specifically, the breccia formation (*M sc*) and both kind of limestones, Viglae (*Js Ks k*) and Pantocrator (*Ji k* and *T5-J3 k*), were classified as ground type A, while the marls from both towns (*M m* and *M m.st*) were classified as type C.

Author Contributions: Conceptualization, J.D.A., N.V., E.V., V.S. and G.K.; methodology, J.D.A., N.V., S.D., E.V., V.S. and G.K.; software, J.D.A., S.D., V.G., I.-K.G. and G.S.M.; validation, J.D.A., S.D., V.G. and I.-K.G.; investigation, J.D.A., N.V., S.D., V.G., I.-K.G. and G.S.M.; resources, J.D.A. and N.V.; data curation, J.D.A., S.D., V.G. and I.-K.G.; writing—original draft preparation, S.D., V.G. and I.-K.G.; writing—review and editing, J.D.A., N.V., S.D., V.S. and G.K.; visualization, J.D.A., S.D., V.G., I.-K.G. and G.S.M.; supervision, J.D.A. and N.V.; funding acquisition, J.D.A. and N.V. All authors have read and agreed to the published version of this manuscript.

Funding: This research was funded by the project “Telemachus - Innovative Seismic Risk Management Operational System of the Ionian Islands” (MIS 5007986) which is part of the Regional Operational Programme «Ionian Islands 2014 2020» and is cofinanced by the European Regional Development Fund (ERDF) (National Strategic Reference Framework NSRF 2014 20).

Data Availability Statement: Data available upon request.

Acknowledgments: The authors would like to thank Petras Athanasios for his valuable contribution during field work and the two anonymous reviewers for their constructive comments that helped improving the initial manuscript.

Conflicts of Interest: The authors declare no conflict of interest.

References

- Ganas, A.; Elias, P.; Bozionelos, G.; Papathanassiou, G.; Avallone, A.; Papastergios, A.; Valkaniotis, S.; Parcharidis, I.; Briole, P. Coseismic deformation, field observations and seismic fault of the 17 November 2015 $M = 6.5$, Lefkada Island, Greece earthquake. *Tectonophysics* **2016**, *687*, 210–222. [[CrossRef](#)]
- Karakostas, V.G.; Papadimitriou, E.E.; Papazachos, C.B. Properties of the 2003 Lefkada, Ionian Islands, Greece, earthquake seismic sequence and seismicity triggering. *Bull. Seismol. Soc. Am.* **2004**, *94*, 1976–1981. [[CrossRef](#)]
- Lekkas, E.; Mavroulis, S.; Carydis, P.; Alexoudi, V. The 17 November 2015 Mw 6.4 Lefkada (Ionian Sea, Western Greece) Earthquake: Impact on Environment and Buildings. *Geotech. Geol. Eng.* **2018**, *36*, 2109–2142. [[CrossRef](#)]
- Papadimitriou, E.; Karakostas, V.; Mesimeri, M.; Chouliaras, G.; Kourouklas, C. The $M_w 6.5$ 17 November 2015 Lefkada (Greece) earthquake: Structural interpretation by means of the aftershock analysis. *Pure Appl. Geophys.* **2017**, *174*, 3869–3888. [[CrossRef](#)]
- Papathanassiou, G.; Pavlides, S.; Ganas, A. The 2003 Lefkada earthquake: Field observations and preliminary microzonation map based on liquefaction potential index for the town of Lefkada. *Eng. Geol.* **2005**, *82*, 12–31. [[CrossRef](#)]
- Sakkas, V.; Kapetanidis, V.; Kaviris, G.; Spingos, I.; Mavroulis, S.; Diakakis, M.; Alexopoulos, J.D.; Kazantzidou-Firtinidou, D.; Kassaras, I.; Dilalos, S.; et al. Seismological and Ground Deformation Study of the Ionian Islands (W. Greece) during 2014–2018, a Period of Intense Seismic Activity. *Appl. Sci.* **2022**, *12*, 2331. [[CrossRef](#)]
- Makropoulos, K.; Kaviri, G.; Kouskouna, V. An updated and extended earthquake catalogue for Greece and adjacent areas since 1900. *Nat. Hazards Earth Syst. Sci.* **2012**, *12*, 1425–1430. [[CrossRef](#)]
- Sakkas, G.; Kouskouna, V.; Makropoulos, K. Seismic hazard analysis in the Ionian Islands using macroseismic intensities. *Hell. J. Geosci.* **2010**, *45*, 239–248.
- Al-Heety, A.J.; Hassouneh, M.; Abdullah, F.M. Application of MASW and ERT methods for geotechnical site characterization: A case study for roads construction and infrastructure assessment in Abu Dhabi, UAE. *J. Appl. Geophys.* **2021**, *193*, 104408. [[CrossRef](#)]
- Cardarelli, E.; Cercato, M.; De Donno, G. Characterization of an earth-filled dam through the combined use of electrical resistivity tomography, P-and SH-wave seismic tomography and surface wave data. *J. Appl. Geophys.* **2014**, *106*, 87–95. [[CrossRef](#)]
- Rezaei, S.; Choobbasti, A.J. Evaluation of local site effect from microtremor measurements in Babol city, Iran. *J. Seismol.* **2017**, *22*, 471–486. [[CrossRef](#)]
- Mohammed, M.A.; Abudeif, A.M.; Abd El-aal, A.K. Engineering geotechnical evaluation of soil for foundation purposes using shallow seismic refraction and MASW in 15th Mayo, Egypt. *J. Afr. Earth Sci.* **2020**, *162*, 103721. [[CrossRef](#)]

13. Pegah, E.; Liu, H. Application of near-surface seismic refraction tomography and multichannel analysis of surface waves for geotechnical site characterizations: A case study. *Eng. Geol.* **2016**, *208*, 100–113. [[CrossRef](#)]
14. Romero-Ruiz, A.; Linde, N.; Keller, T.; Or, D. A review of geophysical methods for soil structure characterization. *Rev. Geophys.* **2018**, *56*, 672–697. [[CrossRef](#)]
15. Salem, H.S. Poisson's ratio and the porosity of surface soils and shallow sediments, determined from seismic compressional and shear wave velocities. *Geotechnique* **2000**, *50*, 461–463. [[CrossRef](#)]
16. Anastasiadis, A.; Margaris, V.; Klimis, N.; Makra, K.; Pitolakis, K. The Lefkada Earthquake (M = 6.2, 14 August 2003): Strong Ground Motion and valuation of the subsoil's impact. In Proceedings of the 5th Panhellenic Conference of Geotechnical & Geoenvironmental Mechanics, Xanthi, Greece, 31 May–2 June 2006. (In Greek).
17. Kassaras, I.; Voulgaris, N.; Makropoulos, K. Determination of Site Response in Lefkada Town (W. Greece) by Ambient Vibration Measurements. In Proceedings of the 31st General Assembly of the European Seismological Commission (ESC), Crete, Greece, 7–12 September 2008; pp. 198–205.
18. Kassaras, I.; Kalantoni, D.; Kouskouna, V.; Pomonis, A.; Michalaki, K.; Stoumpos, P.; Mourloukos, S.; Birpilopoulos, S.; Makropoulos, K. Correlation between damage distribution and soil characteristics deduced from ambient vibrations in the old town of Lefkada (W. Greece). In Proceedings of the 2nd European Conference on Earthquake Engineering and Seismology, Istanbul, Turkey, 25–29 August 2014; pp. 25–29.
19. Kassaras, I.; Kalantoni, D.; Benetatos, C.; Kaviris, G.; Michalaki, K.; Sakellariou, N.; Makropoulos, K. Seismic damage scenarios in Lefkada old town (W. Greece). *Bull. Earthq. Eng.* **2015**, *13*, 3669–3711. [[CrossRef](#)]
20. Gazetas, G. Geotechnical aspects of the Ms 6.4 Lefkada Island, Greece 2003 earthquake: Preliminary assessment. In Proceedings of the 5th International Conference on Case Histories in Geotechnical Engineering, New York, NY, USA, 13–17 April 2004. Paper no. 13.
21. Papanikolaou, D. The tectonostratigraphic terranes of the Hellenides. *Ann. Geol. Pays Hell.* **1997**, *37*, 495–514.
22. Aubouin, J. Contribution a l' etude geologique de la Grece septentrionale, les confins de l' Epire et de la Thessalie. *Ann. Geol. Pays Hell.* **1959**, *10*, 526.
23. Jacobshagen, V. *Geologie von Griechenland*; Beiträge zur regionalen Geologie der Erde; Gebrüder Borntraeger: Stuttgart, Germany, 1986; 363p.
24. Renz, H.H. Some upper Cretaceous and lower Tertiary foraminifera from Aragua and Guarico, Venezuela. *Micropaleontology* **1955**, *1*, 52–63. [[CrossRef](#)]
25. IGME. *Geological Map of Greece, Sheet North Corfu, Scale 1:50.000*; Institute of Geology and Mineral Exploration: Athens, Greece, 1971.
26. Tserolas, P.; Maravelis, A.G.; Tsochandarlis, N.; Pasadakis, N.; Zelilidis, A. Organic geochemistry of the upper Miocene-lower Pliocene sedimentary rocks in the Hellenic Fold and Thrust Belt, NW Corfu island, Ionian sea, NW Greece. *Mar. Pet. Geol.* **2019**, *106*, 17–29. [[CrossRef](#)]
27. Bornovas, J. Géologie de L'île de Lefkade. *Geol. Geophys. Res.* **1964**, *10*, 142. (In French)
28. British Petroleum Company. *The Geological Results of Petroleum Exploration in Western Greece*; Institute of Geology Subsurface Research Athens: Athens, Greece, 1971; Volume 10, 73p.
29. Lekkas, E.; Danamos, G.; Lozios, S. Neotectonic structure and evolution of Lefkada Island. *Bull. Geol. Soc. Greece* **2001**, *34*, 157–163. [[CrossRef](#)]
30. Mitsika, G.S.; Alexopoulos, J.D.; Giannopoulos, I.K.; Gkosios, V.; Dilalos, S.; Filis, C.; Vassilakis, E.; Kaviris, G.; Sakkas, V.; Voulgaris, N. Preliminary results of near-surface geophysical survey in Lefkada town (Greece). In Proceedings of the 16th International Congress of the Geological Society of Greece, Patras, Greece, 17–19 October 2022.
31. IGME. *Geological Map of Greece, Sheet Lefkas, Scale 1:50.000*; Institute of Geology and Mineral Exploration: Athens, Greece, 1963.
32. Adewoyin, O.O.; Joshua, E.O.; Akinyemi, M.L.; Omeje, M.; Adagunodo, T.A. Evaluation of geotechnical parameters of reclaimed land from near-surface seismic refraction method. *Heliyon* **2021**, *7*, e06765. [[CrossRef](#)]
33. Khalil, M.H.; Hanafy, S.M. Engineering applications of seismic refraction method: A field example at Wadi Wardan, Northeast Gulf of Suez, Sinai, Egypt. *J. Appl. Geophys.* **2008**, *65*, 132–141. [[CrossRef](#)]
34. Yilmaz, O.; Eser, M.; Berilgen, M. Seismic, geotechnical, and earthquake engineering site characterization. *SEG Tech. Program Expand. Abstr.* **2006**, *2006*, 1401–1405. [[CrossRef](#)]
35. Zhang, J.; Toksöz, M.N. Nonlinear refraction travelttime tomography. *Geophysics* **1998**, *63*, 1726–1737. [[CrossRef](#)]
36. Zhu, X.; Sixta, D.P.; Angstman, B.G. Tomostatics: Turning-ray tomography+ static corrections. *Lead. Edge* **1992**, *11*, 15–23. [[CrossRef](#)]
37. Stefani, J.P. Turning-ray tomography. *Geophysics* **1995**, *60*, 1917–1929. [[CrossRef](#)]
38. Lanz, E.; Maurer, H.; Green, A.G. Refraction tomography over a buried waste disposal site. *Geophysics* **1998**, *63*, 1414–1433. [[CrossRef](#)]
39. Thurber, C.; Ritsema, J. Theory and observations-seismic tomography and inverse methods. *Seismol. Struct. Earth* **2007**, *1*, 323–360. [[CrossRef](#)]
40. Eker, A.M.; Akgün, H.; Koçkar, M.K. Local site characterization and seismic zonation study by utilizing active and passive surface wave methods: A case study for the northern side of Ankara, Turkey. *Eng. Geol.* **2012**, *151*, 64–81. [[CrossRef](#)]

41. Foti, S.; Parolai, S.; Albarello, D.; Picozzi, M. Application of surface-wave methods for seismic site characterization. *Surv. Geophys.* **2011**, *32*, 777–825. [[CrossRef](#)]
42. Kanlı, A.I.; Tildy, P.; Prónay, Z.; Pinar, A.; Hermann, L. V_S^{30} mapping and soil classification for seismic site effect evaluation in Dinar region, SW Turkey. *Geophys. J. Int.* **2006**, *165*, 223–235. [[CrossRef](#)]
43. Karabulut, S. Soil classification for seismic site effect using MASW and ReMi methods: A case study from western Anatolia (Dikili-İzmir). *J. Appl. Geophys.* **2018**, *150*, 254–266. [[CrossRef](#)]
44. Socco, L.V.; Strobbia, C. Surface-wave method for near-surface characterization: A tutorial. *Near Surf. Geophys.* **2004**, *2*, 165–185. [[CrossRef](#)]
45. Xia, J.; Miller, R.D.; Park, C.B.; Hunter, J.A.; Harris, J.B.; Ivanov, J. Comparing shear-wave velocity profiles inverted from multichannel surface wave with borehole measurements. *Soil Dyn. Earthq. Eng.* **2002**, *22*, 181–190. [[CrossRef](#)]
46. Park, C.B.; Miller, R.D.; Xia, J. Offset and resolution of dispersion curve in multichannel analysis of surface waves (MASW). In *Symposium on the Application of Geophysics to Engineering and Environmental Problems 2001*; SSM4-SSM4; Society of Exploration Geophysicists: Tulsa, OK, USA, 2001. [[CrossRef](#)]
47. Geometrics Inc.; OYO Inc. *SeisImager Manual, Version 3.3*; Computer Program Manual; OYO Corporation: Tokyo, Japan, 2009.
48. Babuska, V.; Cara, M. *Seismic Anisotropy in the Earth*; Kluwer Academic Publishers: Boston, MA, USA, 1991.
49. Park, C.B.; Miller, R.D.; Xia, J. Multichannel analysis of surface waves. *Geophysics* **1999**, *64*, 800–808. [[CrossRef](#)]
50. European Committee for Standardization. *EN-1998-1, Eurocode 8; Design of Structures for Earthquake Resistance”, Part 1: General Rules*; European Committee for Standardization: Brussels, Belgium, 2004.
51. Abzalov, M.Z. Measuring and modelling of dry bulk rock density for mineral resource estimation. *Applied Earth Science* **2013**, *122*, 16–29. [[CrossRef](#)]
52. Dilalos, S. Application of Geophysical Technique to the Investigation of Tectonic Structures in Urban and Suburban Environments. A Case Study in Athens Basin. Ph.D. Thesis, National and Kapodistrian University of Athens, Athens, Greece, 2018. Available online: <http://hdl.handle.net/10442/hedi/48791> (accessed on 25 September 2022).
53. Dilalos, S.; Alexopoulos, J.D.; Lozios, S. New insights on Athens basin (Greece) subsurface geological and tectonic structure, derived from urban gravity measurements. *J. Appl. Geophys.* **2019**, *167*, 73–105. [[CrossRef](#)]
54. Dilalos, S.; Alexopoulos, J.D.; Vassilakis, E.; Poulos, S.E. Investigation of the structural control of a deltaic valley with geophysical methods. The case study of Pineios river delta (Thessaly, Greece). *J. Appl. Geophys.* **2022**, *202*, 104652. [[CrossRef](#)]
55. García-Pérez, T.; Marquardt, C.; Yáñez, G.; Cembrano, J.; Gomila, R.; Santibañez, I.; Maringue, J. Insights on the structural control of a Neogene forearc basin in Northern Chile: A geophysical approach. *Tectonophysics* **2018**, *736*, 1–14. [[CrossRef](#)]
56. Parasnis, D.S. A study of rock densities in the English Midlands. *Geophys. Suppl. Mon. Not. R. Astron. Soc.* **1952**, *6*, 252–271. [[CrossRef](#)]
57. Basheer, A.A.; Salama, N.S. Application of ERT and SSR for geotechnical site characterization: A case study for resort assessment in New El Alamein City, Egypt. *NRIAG J. Astron. Geophys.* **2022**, *11*, 58–68. [[CrossRef](#)]
58. Elkafrawy, S.B.; Fattah, T.A.; Naiel, T.; Rashed, M.; Abbas, A.M. Environmental and site characterization investigations using remote sensing and geophysical techniques—A case from Nabq, Gulf of Aqaba, Sinai, Egypt. *Remote Sens. Appl. Soc. Environ.* **2021**, *24*, 100653. [[CrossRef](#)]
59. Fat-Helbary, R.E.S.; El-Faragawy, K.O.; Hamed, A. Soil geotechnical characteristics for seismic risk mitigation at the southern extension of Marsa Alam city, Egypt. *NRIAG J. Astron. Geophys.* **2019**, *8*, 1–14. [[CrossRef](#)]
60. Gkosios, V.; Alexopoulos, J.D.; Giannopoulos, I.K.; Mitsika, G.S.; Dilalos, S.; Barbaresos, I.; Voulgaris, N. Determination of the subsurface geological regime and geotechnical characteristics at the area of Goudi (Athens, Greece) derived from geophysical measurements. Bulletin of the Geological Society of Greece, Special Publication GSG2022-062. In Proceedings of the 16th International Congress of the Geological Society of Greece, Patras, Greece, 17–19 October 2022.
61. Razmyar, A.; Eslami, A. Evaluating the geotechnical and geophysical characteristics of expanding districts in Tehran using field experiments. *Civ. Eng. J.* **2018**, *4*, 363–377. [[CrossRef](#)]
62. Adams, L.H. Elastic Properties of Materials of the Earth’s Crust. In *Internal Construction of the Earth*; Gutenberg, B., Ed.; Dover Publications, Inc.: New York, NY, USA, 1951.
63. Toksöz, M.N.; Cheng, C.H.; Timur, A. Velocities of seismic waves in porous rocks. *Geophysics* **1976**, *41*, 621–645. [[CrossRef](#)]